arXiv:1601.00468v2 [physics.chem-ph] 3 Feb 2016

Curvature-dependence of the liquid-vapor surface tension beyond the Tolman approximation

Nicolas Bruot and Frédéric Caupin
Institut Lumière Matière, UMR5306 Université Claude Bernard Lyon 1 — CNRS, Université de Lyon, Institut Universitaire de France, 69622 Villeurbanne cedex, France

Surface tension is a macroscopic manifestation of the cohesion of matter, and its value σ_∞ is readily measured for a flat liquid-vapor interface. For interfaces with a small radius of curvature R, the surface tension might differ from σ_∞. The Tolman equation, $\sigma(R) = \sigma_\infty/(1 + 2\delta/R)$, with δ a constant length, is commonly used to describe nanoscale phenomena such as nucleation. Here we report experiments on nucleation of bubbles in ethanol and n-heptane, and their analysis in combination with their counterparts for the nucleation of droplets in supersaturated vapors, and with water data. We show that neither a constant surface tension nor the Tolman equation can consistently describe the data. We also investigate a model including $1/R$ and $1/R^2$ terms in $\sigma(R)$. We describe a general procedure to obtain the coefficients of these terms from detailed nucleation experiments. This work explains the conflicting values obtained for the Tolman length in previous analyses, and suggests directions for future work.

Accepted to Physical Review Letters.

Nucleation in metastable phases is an ubiquitous phenomenon, relevant to important fields such as atmospheric research [1], mechanics of plants and trees [2–4], and in the chemical industry to avoid vapor explosions accidents (or "spill accidents") [5]. The nucleation rate is exquisitely sensitive to the value of the surface tension σ between the metastable and the stable phase. As the size of the critical nucleus that triggers the phase change is in the nanometer range, the value of σ relevant to nucleation may differ from the bulk one. The idea of a dependence of the surface tension on the curvature of the interface between phases has been studied by Tolman [6], who proposed for a spherical droplet with radius R

$$\frac{\sigma_\infty}{\sigma(R)} = 1 + \frac{2\delta_\infty}{R}\,, \tag{1}$$

where δ_∞ is the Tolman length. Determining in experiments $\sigma(R)$ is critical to developing accurate nucleation theories. It can also serve as an input to validity checks of density functional theory calculations and numerical simulations. More generally, the small scale limit at which macroscopic laws break down is an active field of research, as shown for instance by recent studies on vapor pressure of nanodroplets [7], or on flows in nanochannels [8], that are of crucial importance for oil recovery and catalysis.

The curvature dependence of surface tension has been mainly studied theoretically and numerically, with conflicting results about the magnitude and even the sign of the effect [6, 9–18]. The dearth of experimental data stems from the difficulties inherent to measurements on nanoscopic objects. In this work we circumvent this problem by use of the nucleation theorem (NT) [19, 20], which allows obtaining information on the nanoscopic critical nucleus from a macroscopic observable, the nucleation rate (number of nucleation events per unit volume and time). In addition, we adopt a comprehensive approach, treating on the same footing the two symmetric cases of nanodroplets (related to the nucleation of a liquid from a supersaturated vapor, condensation) and nanobubbles (related to the nucleation of a vapor in a metastable liquid, cavitation). To complement existing data on condensation, we have performed acoustic cavitation experiments on ethanol and heptane.

In acoustic cavitation, the liquids are stretched using a few cycles of a focused acoustic wave at 1 MHz to trigger nucleation (see [21] and Supplemental Material, SM, for details). The wave frequency sets the experimental time and volume, and consequently the observable nucleation rate. The pressure at which this rate is reached is shown in Fig. 1(a) for ethanol and in Fig. S1(a) of the SM for heptane. Compared to a previous study where the cavitation pressures were based on an indirect estimate [22], we have now measured them directly with a fiber-optic probe hydrophone (FOPH) [23]. These more accurate measurements lead to lower pressures than the previous study, as expected because of the nonlinearities in the acoustic wave (see SM and [24, 25]).

An excellent introduction to the concept of curvature-dependent surface tension can be found in [10]. We just introduce here the relevant quantities on the example of condensation. Consider a small spherical droplet of liquid in equilibrium with its supersaturated vapor at chemical potential μ. The pressure of the bulk liquid and vapor at μ are P_L and P_V, and their densities ρ_L and ρ_V, respectively. The key point is that the surface tension σ depends on the radius R chosen for the dividing sphere which separates by convention the liquid and vapor regions. Two radii are of particular interest in describing the droplet. The first is R_e, the radius of the equimolar dividing surface. The second is R_s, the radius of the sphere at which the Laplace relation is fulfilled:

$$\Delta P = P_\mathrm{L} - P_\mathrm{V} = \frac{2\sigma_\mathrm{s}}{R_\mathrm{s}}\,, \tag{2}$$

where $\sigma_\mathrm{s} = \sigma(R_\mathrm{s})$. R_s allows to write the energy barrier

for nucleation $\Delta\Omega$ in a compact form:

$$\Delta\Omega = \frac{4\pi}{3} R_s^2 \sigma_s = \frac{16\pi\sigma_s^3}{3\Delta P^2} \,. \tag{3}$$

In classical nucleation theory (CNT), the nucleation rate J for the phase change is

$$J = J_0 \exp\left(-\frac{\Delta\Omega}{k_B T}\right) \,, \tag{4}$$

with J_0 a prefactor, whose expression is given in the SM. The knowledge of J at a given μ or ΔP (the quantity controlled in an experiment) thus gives access to $\Delta\Omega$ from Eq. (4), σ_s from Eq. (3) and R_s^* from Eq. (2). Starred quantities are relative to the critical nucleus, at which the energy barrier $\Delta\Omega$ is reached. In addition, experiments can give access to R_e^* [19, 20]. Indeed, if the dependence of J on μ is known, the excess number of molecules in the critical nucleus is

$$\Delta n^* = k_B T \left(\frac{\partial \ln(J/J_0)}{\partial \mu}\right)_T \,. \tag{5}$$

For $\rho_V \ll \rho_L$, and assuming a spherical critical droplet whose density at the center reaches the bulk value, this leads to an expression for the volume of the sphere with radius R_e^* (see SM):

$$V_e^* = \frac{4\pi}{3} R_e^{*3} = \frac{|\Delta n^*|}{\rho_L} = \frac{k_B T}{\rho_L} \left|\left(\frac{\partial \ln(J/J_0)}{\partial \mu}\right)_T\right| \,. \tag{6}$$

Eqs. (3) to (6) hold for both cavitation and condensation, provided that adequate expressions for ΔP, μ and J_0 are used.

To test different models for the surface tension, we have used experimental values of J at known μ (condensation data), or, equivalently, ΔP at fixed J (cavitation data), and V_e^* . The models are described below and are summarized in Table I.

In the standard version of the CNT [26], CNT_0, σ_s is assumed to always remain equal to the value for a planar interface σ_∞, which is equivalent to setting $R_e = R_s$, and $\Delta\Omega = 16\pi{\sigma_\infty}^3/(3\Delta P^2)$. CNT_0 is notorious to fail in predicting correct nucleation rates, for cavitation [27] as well as for condensation [14, 28–35]. This appears clearly in Figs. 1 and S1, where the FOPH experiments are plotted along with condensation data [28, 31, 32, 36–40], and with a cavitation point from a water inclusion in quartz [27]. For instance, Figs. 1(b) and S1(b,d) highlight for the three fluids a crossover temperature below which CNT_0 underestimates the condensation rates, and above which they are overestimated. This crossover had already been observed in single data sets for ethanol and water condensation, e.g. [32] and [41], and the combination of several sets makes this conclusion stronger.

We therefore investigate other models with $R_e \neq R_s$. We use a functional form suggested by simulations [10]:

$$\delta(R_s) = \delta_\infty + \frac{\alpha}{R_s} \,. \tag{7}$$

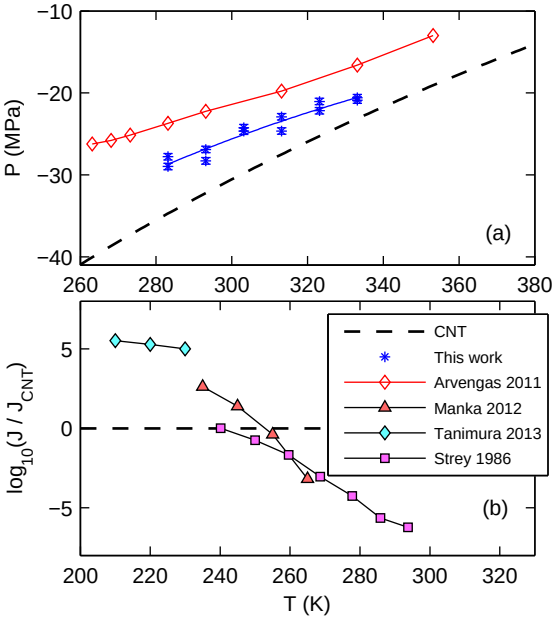

FIG. 1. Comparison of nucleation pressures or rates (markers) with CNT_0 (dashed lines) in ethanol. (a) Acoustic cavitation pressures obtained with the FOPH (blue stars) are compared to previous pressure estimates (red diamonds) via a static pressure method [22]. The new, more accurate points are consistently more negative, as expected (see SM). The blue line is a guide to the eye. (b) Condensation data. Each graph represents the logarithm of the ratio between the nucleation rate and the CNT_0 prediction. The data sources are indicated in the legend. See Fig. S1 in the SM for the corresponding graphs for heptane and water.

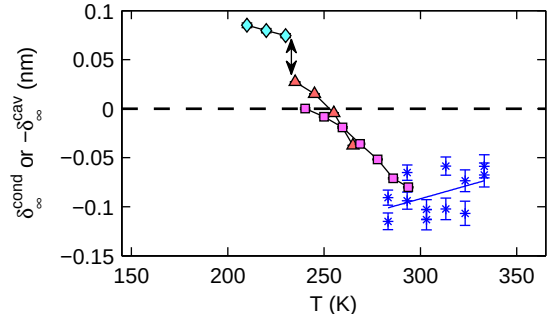

FIG. 2. δ_∞ depending on temperature for cavitation (star markers) and condensation (filled markers) in ethanol. The legend is the same as in Fig. 1. The double arrows point to discrepancies that suggest the failure of the CNT_1 model: δ_∞, which is expected to be the Tolman length, would not only depend on T. The blue line is a guide to the eye of the FOPH data. See Fig. S2 for heptane and water.

Starting with a first variant of CNT, CNT_1, which assumes $\alpha = 0$ in Eq. (7), it can be shown that [10]

$$\frac{\sigma_\infty}{\sigma_s} = 1 + \frac{2\delta_\infty}{R_s} + \mathcal{O}\left(\frac{1}{{R_s}^2}\right) \,, \tag{8}$$

which is similar to Eq. (1). One can then calculate δ_∞

Model	Surface tension	Free parameters	Input data
CNT_0	$\sigma(R_s) = \sigma_\infty$	None	None
CNT_1	$\frac{\sigma_\infty}{\sigma(R_s)} = 1 + \frac{2\delta_\infty}{R_s}$	δ_∞	J
CNT_2	$\frac{\sigma_\infty}{\sigma(R_s)} = 1 + \frac{2\delta_\infty}{R_s} + \frac{\delta_\infty^2 + \alpha}{R_s^2}$	δ_∞ and $\delta_\infty^2 + \alpha$	J and V_e^*

TABLE I. Summary of the models tested in this Letter. For each model, we indicate the expression for the surface tension, the free parameters and the experimental data used to extract these parameters.

from the experimental nucleation rates (see SM). The analysis usually stops there [11, 27, 31], which does not provide a full test of CNT_1. We take a step further, and predict V_e^* from δ_∞ with CNT_1 (see SM). A comparison between predicted V_e^* and V_e^* deduced from the experiments with the NT Eq. (6) becomes possible. To our knowledge, this type of reasoning has been employed only for water [27, 31], with a seemingly satisfactory agreement. By a more comprehensive analysis of all the data sets gathered for ethanol, heptane and water, covering a broader range for temperature and degree of metastability, we find discrepancies that reveal the actual failure of CNT_1. Figs. 2 and S2 show δ_∞ calculated from the cavitation and condensation experiments. Quantities relative to cavitation and condensation are labelled by 'cav' or 'cond', respectively. If CNT_1 were valid, we would expect to find that $\delta_\infty^{\rm cav}$ and $\delta_\infty^{\rm cond}$ do not depend on R_s^* and that $\delta_\infty^{\rm cav} = -\delta_\infty^{\rm cond}$ for the same temperatures [10]. For each of the fluids, the points do not collapse on a single curve, as indicated by the double arrows, even when taking into account the experimental uncertainties (see SM for details). This suggests that δ does in fact depend on R_s^*. We emphasize that the disagreement can usually not be seen when looking at the data of a single condensation experiment. This is because various independent supersaturation and temperature values are needed to conclude and the combination of several condensation and cavitation experiments extends the range of both parameters. The crossover mentioned earlier translates here into a change of $\delta_{\rm cond}$ from positive to negative values when T increases (Figs. 2 and S2). This behavior is not in support of CNT_1. The situation gets even worse when comparing in Figs. 3 and S3 V_e^* extracted from this model (small, light markers) with V_e^* obtained using the NT (big, dark markers). In overall, these agree at low temperature, but strongly disagree above 250-300 K depending on the fluid. We note that the approximations needed to deduce V_e^* from experiments with Eq. (6) lead to an underestimate of V_e^* for both cavitation and condensation, so that the disagreement with CNT_1 can be only stronger than shown in Figs. 3 and S3. Also, the critical volumes for cavitation may display a systematic error bigger than the statistical error bars shown here because of an extrapolation in the data analysis. All these details are investigated in the SM and Refs. [42, 43] and do not change any of our conclusions.

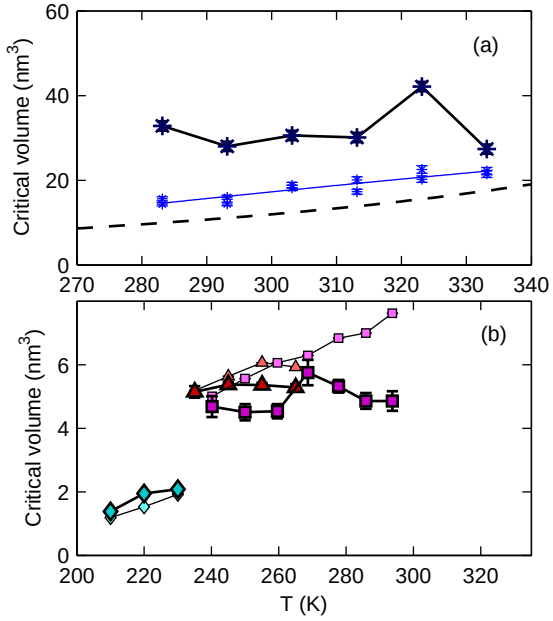

FIG. 3. Critical volumes in (a) cavitation and (b) condensation experiments for ethanol. The thick and thin markers represent the volumes from the NT and from CNT_1, respectively. The legend is the same as in Fig. 1. See Fig. S3 for heptane and water.

We now move on to a second variant of CNT, CNT_2, based on Eq. (7) with two parameters δ_∞ and $\alpha \neq 0$. It can then be shown that [44]:

$$\frac{\sigma_\infty}{\sigma_s} = 1 + \frac{2\delta_\infty}{R_s} + \frac{{\delta_\infty}^2 + \alpha}{{R_s}^2} + \mathcal{O}\left(\frac{1}{{R_s}^3}\right). \qquad (9)$$

It may seem that adding an extra parameter would automatically allow a better fitting of the data. But we also use more experimental input (see Table I). For CNT_1, we used only the experimental nucleation rates to calculate δ_∞, and compared the CNT_1 prediction for V_e^* with the values from experiments on which the nucleation theorem can be applied. For CNT_2, we use both the nucleation rates and V_e^* from those experiments to directly calculate δ_∞ and $\delta_\infty^2 + \alpha$ (see SM). The success of the approach must therefore be assessed by checking if

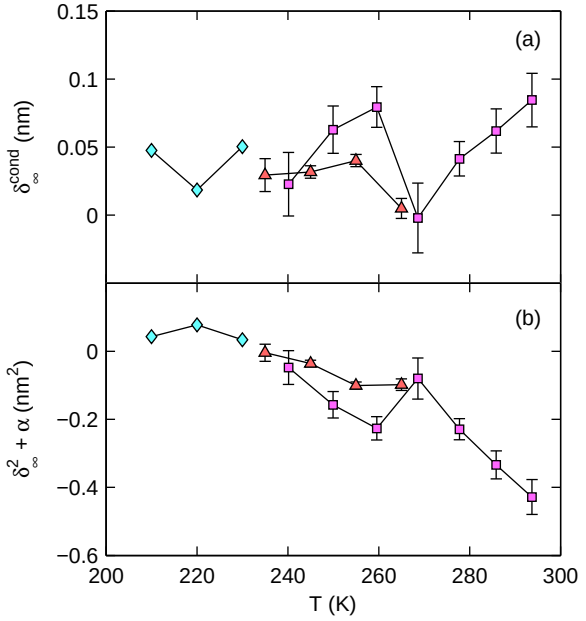

FIG. 4. CNT_2 parameters δ_∞ and $\delta_\infty^2 + \alpha$ derived from condensation experiments. See Fig. 1 for the legend, and Fig. S4 for heptane and water.

the various data sets lead to master curves for both δ_∞ *and* $\delta_\infty^2 + \alpha$ as a function of the temperature. The results are plotted in Figs. 4 and S4. We have omitted here the FOPH data, since, unfortunately, the corresponding error bars on δ_∞ and $\delta_\infty^2 + \alpha$ would be of the order of the size of the y-axes (see SM). For heptane, only one data set is available and does not allow to test the data collapse. For the other fluids, we observe a more consistent description of the data (see in particular the improvement of the discrepancy between the Tanimura 2013 and the Manka 2012 data compared to Fig. 2). The agreement is still not perfect, even when taking into account the statistical uncertainties on the points. This is possibly indicative of systematic errors specific to the different experiments, or of some limitation of the theory, such as that of a spherical critical nucleus. Compared to CNT_1, CNT_2 yields a Tolman length δ_∞ with a weaker temperature dependence, and for ethanol and water δ_∞ now keeps a positive sign. For heptane, δ_∞ is close to zero, maybe slightly negative. For the three fluids, we noted that the second order term $(\delta_\infty^2 + \alpha)/(R_s^*)^2$ is often of the same order of magnitude as the first order term δ_∞/R_s^* (see SM).

Our results show that, at least for ethanol, heptane and water, the usual Tolman equation Eq. (1) is not enough to properly describe experiments. Therefore, attempts to analyse experiments with CNT_1 (such as in [11, 27, 31]) may yield inaccurate determinations of δ_∞, and this study partly explains the confusion in the longstanding debate on the sign of the Tolman length [45]. The CNT_2 approach seems to give more consistent results.

A variety of simulations have been realized and motivated our work. We have tried to compare the experiments to these. For heptane, the δ_∞^{cond} we found is close to zero and possibly negative (around -0.02 nm). An expression of the Tolman length as a function of the isothermal compressibility κ_T has been proposed [46, 47]: $\delta_\infty = -\kappa_T \sigma_\infty$. At 265 K, the formula yields $\delta_\infty \approx -0.03$ nm for heptane, which is close to the experiments in Fig. S4(a). Heptane may be crudely approximated by a Lennard-Jones fluid, for which DFT calculations and MC simulations [9, 10] seem to point to a slightly negative value for δ_∞^{cond} (-0.07 nm). However, MD simulations [44] find a positive temperature-dependent $-\delta_\infty^{cav}$ ($+0.1$ nm at 265 K). Also, Iwamastu [48] estimated the Tolman length from the correlation lengths of the liquid and vapor phases, which for heptane translates into $\delta_\infty^{cond} \approx -0.2$ nm, which has a larger magnitude than the experimental value. The parameter $\delta_\infty^2 + \alpha$ has been estimated by MD simulations [44] and by DFT [9, 49]. Rescaled to heptane, these estimates all lead to a positive $(\delta_\infty^2 + \alpha)/R_s^2$ of about 0.4 [44], while the Rudek data set displays mostly negative values: $(\delta_\infty^2 + \alpha)/R_e^2 = -0.1$ in average in the 250-275 K range. By identifying Eq. (9) to the Helfrich form of the surface free energy in Ref. [50], we find the average curvature-elastic moduli $2k_c + \bar{k}_c = 7 \times 10^{-22}$ J.

For the other fluids, the different experiments partially collapse on master curves, thus supporting the CNT_2 model, but they can hardly be compared to simulations or DFT estimates based on the Lennard-Jones potential. For water, we first note that within CNT_2, the cavitation [27] and the condensation [40] experiments yield to positive δ_∞^{cond} or $-\delta_\infty^{cav}$. This sign is consistent with simulations based on a monoatomic model of water (mW) where a departure from the Kelvin equation is observed at small droplet radii [7]. However, the CNT_2 analysis of two simulations with TIP4P/2005 [11, 51] would give the opposite sign: $\delta_\infty^{cond} = -0.066$ nm at 300 K for [11] that measured directly the radius-dependence of the surface free energy of droplets, and $-\delta_\infty^{cav} = -0.067$ nm for the cavitation simulations in [51] from which we have calculated δ_∞ with the energy barrier and the critical volume (using the data from their "M-method" to estimate V_e^*).

While our conclusions on the inaccuracy of the CNT_1 model are unambiguous — we strongly recommend not to use the Tolman equation when analysing nucleation data —, they call for further experiments to confirm the CNT_2 model. As the vapor supersaturation can be varied over a broad range in experiments on condensation, they should be more appropriate than cavitation. For ethanol, the success of CNT_2 is already very promising, and we provide in the SM overall fitting parameters for δ_∞ and $\delta_\infty^2 + \alpha$ that can be used to predict the nucleation rate from any condition. For other fluids, our study provides a procedure with which future measurements of nucleation rates and critical volumes can be analysed.

ACKNOWLEDGMENTS

We acknowledge funding by the ERC under the European FP7 Grant Agreement 240113, and by the Agence Nationale de la Recherche Grant 09-BLAN-0404-01.

[1] B. J. Murray, D. O'Sullivan, J. D. Atkinson, and M. E. Webb, Chem. Soc. Rev. **41**, 6519 (2012).
[2] Y. Forterre, J. Exp. Bot. (2013).
[3] X. Noblin, N. O. Rojas, J. Westbrook, C. Llorens, M. Argentina, and J. Dumais, Science **335**, 1322 (2012).
[4] T. D. Wheeler and A. D. Stroock, Nature **455**, 208 (2008).
[5] P. G. Debenedetti, *Metastable Liquids* (Princeton University Press, 1996).
[6] R. C. Tolman, J. Chem. Phys. **17**, 333 (1949).
[7] M. H. Factorovich, V. Molinero, and D. A. Scherlis, J. Am. Chem. Soc. **136**, 4508 (2014).
[8] P. Huber, J. Phys.: Condens. Matter **27**, 103102 (2015).
[9] B. J. Block, S. K. Das, M. Oettel, P. Virnau, and K. Binder, J. Chem. Phys. **133**, 154702 (2010).
[10] A. Tröster, M. Oettel, B. Block, P. Virnau, and K. Binder, J. Chem. Phys. **136**, 064709 (2012).
[11] M. N. Joswiak, N. Duff, M. F. Doherty, and B. Peters, J. Phys. Chem. Lett. **4**, 4267 (2013).
[12] J. Hrubý, D. G. Labetski, and M. E. H. van Dongen, J. Chem. Phys. **127**, 164720 (2007).
[13] T. V. Bykov and X. C. Zeng, J. Chem. Phys. **111**, 3705 (1999).
[14] T. P. Bennett and J. C. Barrett, J. Chem. Phys. **137**, 124702 (2012).
[15] A. E. van Giessen and E. M. Blokhuis, J. Chem. Phys. **131**, 164705 (2009).
[16] M. Horsch, H. Hasse, A. K. Shchekin, A. Agarwal, S. Eckelsbach, J. Vrabec, E. A. Müller, and G. Jackson, Phys. Rev. E **85**, 031605 (2012).
[17] E. Santiso and A. Firoozabadi, AIChE J. **52**, 311 (2006).
[18] M. P. Moody and P. Attard, Phys. Rev. Lett. **91**, 056104 (2003).
[19] D. W. Oxtoby and D. Kashchiev, J. Chem. Phys. **100**, 7665 (1994).
[20] D. Kashchiev, J. Chem. Phys. **125**, 014502 (2006).
[21] E. Herbert, S. Balibar, and F. Caupin, Phys. Rev. E **74**, 041603 (2006).
[22] A. Arvengas, E. Herbert, S. Cersoy, K. Davitt, and F. Caupin, J. Phys. Chem. B **115**, 14240 (2011).
[23] A. Arvengas, K. Davitt, and F. Caupin, Rev. Sci. Instrum. **82**, 034904 (2011).
[24] C. Appert, C. Tenaud, X. Chavanne, S. Balibar, F. Caupin, and D. d'Humiéres, Eur. Phys. J. B **35**, 531 (2003).
[25] K. Davitt, E. Rolley, F. Caupin, A. Arvengas, and S. Balibar, J. Chem. Phys. **133**, (2010).
[26] P. G. Debenedetti, "Metastable liquids," (Princeton University Press, 1996) Chap. Kinetics, pp. 148–234.
[27] M. E. M. Azouzi, C. Ramboz, J.-F. Lenain, and F. Caupin, Nat. Phys. **9**, 38 (2013).
[28] D. Ghosh, D. Bergmann, R. Schwering, J. Wlk, R. Strey, S. Tanimura, and B. E. Wyslouzil, J. Chem. Phys. **132**, 024307 (2010).
[29] Y. J. Kim, B. E. Wyslouzil, G. Wilemski, J. Wölk, and R. Strey, J. Phys. Chem. A **108**, 4365 (2004).
[30] C. C. M. Luijten, K. J. Bosschaart, and M. E. H. van Dongen, J. Chem. Phys. **106**, 8116 (1997).
[31] V. Holten, D. G. Labetski, and M. E. H. van Dongen, J. Chem. Phys. **123**, 104505 (2005).
[32] A. A. Manka, J. Wedekind, D. Ghosh, K. Höhler, J. Wölk, and R. Strey, J. Chem. Phys. **137**, 054316 (2012).
[33] A.-P. Hyvärinen, H. Lihavainen, Y. Viisanen, and M. Kulmala, J. Chem. Phys. **120**, 11621 (2004).
[34] P. Peeters, J. J. H. Gielis, and M. E. H. van Dongen, J. Chem. Phys. **117**, 5647 (2002).
[35] J. A. Fisk and J. L. Katz, J. Chem. Phys. **104**, 8649 (1996).
[36] S. Tanimura, H. Pathak, and B. E. Wyslouzil, J. Chem. Phys. **139**, 174311 (2013).
[37] R. Strey, P. E. Wagner, and T. Schmeling, J. Chem. Phys. **84**, 2325 (1986).
[38] M. M. Rudek, J. A. Fisk, V. M. Chakarov, and J. L. Katz, J. Chem. Phys. **105**, 4707 (1996).
[39] J. Wölk and R. Strey, J. Phys. Chem. B **105**, 11683 (2001).
[40] D. Brus, V. Ždímal, and J. Smolík, J. Chem. Phys. **129**, 174501 (2008).
[41] V. B. Mikheev, P. M. Irving, N. S. Laulainen, S. E. Barlow, and V. V. Pervukhin, J. Chem. Phys. **116**, 10772 (2002).
[42] D. W. Oxtoby, Acc. Chem. Res. **31**, 91 (1998).
[43] D. Kashchiev, J. Chem. Phys. **118**, 1837 (2003).
[44] V. G. Baidakov and K. S. Bobrov, J. Chem. Phys. **140**, 184506 (2014).
[45] A. Malijevský and G. Jackson, J. Phys.: Condens. Matter **24**, 464121 (2012).
[46] L. S. Bartell, J. Phys. Chem. B **105**, 11615 (2001).
[47] E. M. Blokhuis and J. Kuipers, J. Chem. Phys. **124**, (2006).
[48] M. Iwamatsu, J. Phys.: Condens. Matter **6**, L173 (1994).
[49] E. M. Blokhuis and A. E. van Giessen, J. Phys.: Condens. Matter **25**, 225003 (2013).
[50] W. Helfrich, Z. Naturforsch. C **28**, 693 (1973).
[51] M. A. González, G. Menzl, J. L. Aragones, P. Geiger, F. Caupin, J. L. F. Abascal, C. Dellago, and C. Valeriani, J. Chem. Phys. **141**, 18C511 (2014).

arXiv:1601.00468v2 [physics.chem-ph] 3 Feb 2016

Supplemental Material for Curvature-dependence of the liquid-vapor surface tension beyond the Tolman approximation

Nicolas Bruot and Frédéric Caupin
Institut Lumière Matière, UMR5306 Université Claude Bernard Lyon 1-CNRS, Université de Lyon and Institut Universitaire de France, 69622 Villeurbanne cedex, France

This note provides additional information on the experiments and the analysis presented in the Letter, and presents an analysis of n-heptane and water nucleation data to complement the ethanol data. It also discusses the uncertainties and approximations to support our conclusions. When not specified, the notations and legends in this document are the same as in the main text.

Contents

I. Materials and methods 2

II. Comparison between the static pressure and FOPH methods 2

III. Study of n-heptane and water 2

IV. Formula of the modified CNTs 2
A. $\mathrm{CNT}_\mathbf{1}$ 2
B. $\mathrm{CNT}_\mathbf{2}$ 4
C. Choice for the kinetic prefactor 4
1. Cavitation 4
2. Condensation 4
D. Derivation of the critical volumes from the nucleation theorem 4

V. Effect of the extrapolation of the voltage to pressure relation (cavitation experiments) 6

VI. $\mathrm{CNT}_\mathbf{2}$ for cavitation 8

VII. Estimate of the statistical error bars 8
A. Fiber-optic probe hydrophone experiments 8
B. Condensation experiments 9

VIII. Second order approximation for the surface tension $\boldsymbol{\sigma_\mathrm{s}}$ 10
A. Validity 10
B. Comparison of the two terms in the $\boldsymbol{\sigma}_\mathrm{s}$ expansion of the $\mathrm{CNT}_\mathbf{2}$ 10

IX. Fitted $\mathrm{CNT}_\mathbf{2}$ parameters for ethanol 11

References 11

I. MATERIALS AND METHODS

We have performed acoustic cavitation in n-heptane (Sigma Aldrich, puriss. p.a., $\geq$ 99%) and ethanol (VWR Prolabo Chemicals, 99.98% v/v), using a hemispherical piezoelectric transducer to focus 1 MHz sound bursts (a few cycles long) in a small region of the liquid far from any wall[1]. Ramping the excitation voltage of the transducer, the cavitation probability increases from 0 to 1. The "cavitation threshold" corresponds to a 50% cavitation probability during a burst. In a previous study[2], the pressure at the focus was estimated indirectly by studying the effect of the static pressure in the liquid on the cavitation threshold. Here, we have measured the density of the fluid at the focus directly with a fiber-optic probe hydrophone[3], which is sensitive to the modulation of the refractive index by the sound wave. To convert the density into a pressure, we used an equation of state for the liquid at positive pressure, and extrapolated it down to about -30 MPa. More details will be given elsewhere.

II. COMPARISON BETWEEN THE STATIC PRESSURE AND FOPH METHODS

Figs. 1(a) and S1(a) show pressures at the cavitation threshold slightly more negative with the FOPH than the previously reported values. Here we give an explanation for the discrepancy.

The static pressure method in Ref. 2 was based on the dependence of the transducer voltage at the cavitation threshold on the positive static pressure applied to the liquid. A linear extrapolation gave an indirect estimate of the negative cavitation pressure. However, nonlinearities lead to extrapolated pressures less negative than the real ones[4]. The new experiments with a FOPH give direct access to the density of the liquid at the cavitation threshold. The only remaining assumption resides here in the conversion of the density into a pressure, that requires to extrapolate to negative pressure an equation of state measured at positive pressure. In the case of water, we have previously measured the equation of state at negative pressure and proven that this assumption is valid[5]. It is reasonable to assume that the extrapolation would also be valid for heptane and ethanol, thus yielding to FOPH points that are more accurate than the points from the static pressure method.

III. STUDY OF n-HEPTANE AND WATER

The analysis carried in the Letter on ethanol can be extended to other liquids. Figures S1, S2, S3, S4 below show results for n-heptane and water.

IV. FORMULA OF THE MODIFIED CNTS

This sections gives the formula we have used to calculate the CNT_1 and CNT_2 parameters, and the critical volumes from the nucleation theorem.

A. CNT_1

In the CNT_1, Eq. (8) is written at the critical radius, $R_\mathrm{s} = R_\mathrm{s}^*$. R_s^* is trivially deduced from the Laplace equation as a function of the energy barrier $\Delta\Omega$, and ΔP, that are known from the experiments:

$$R_\mathrm{s}^* = \left(\frac{3\Delta\Omega}{2\pi\Delta p}\right)^{1/3} \tag{S1}$$

Since Eq. (3) with $R_\mathrm{s} = R_\mathrm{s}^*$ links $\sigma_\mathrm{s}(R_\mathrm{s}^*)$ to $\Delta\Omega$ and R_s^*, we obtain the following expression for the Tolman length:

$$\delta_\infty = \frac{\sigma_\infty}{\Delta P}\left[1 - \left(\frac{3\Delta\Omega}{16\pi\sigma_\infty^3}\right)^{1/3}\right] \tag{S2}$$

Compared to CNT_0, the critical equimolar radius now depends on δ_∞. The derivation is done in Ref. 6 and gives

$$R_\mathrm{e}^* = \frac{2\sigma_\infty}{\Delta P} - \delta_\infty \tag{S3}$$

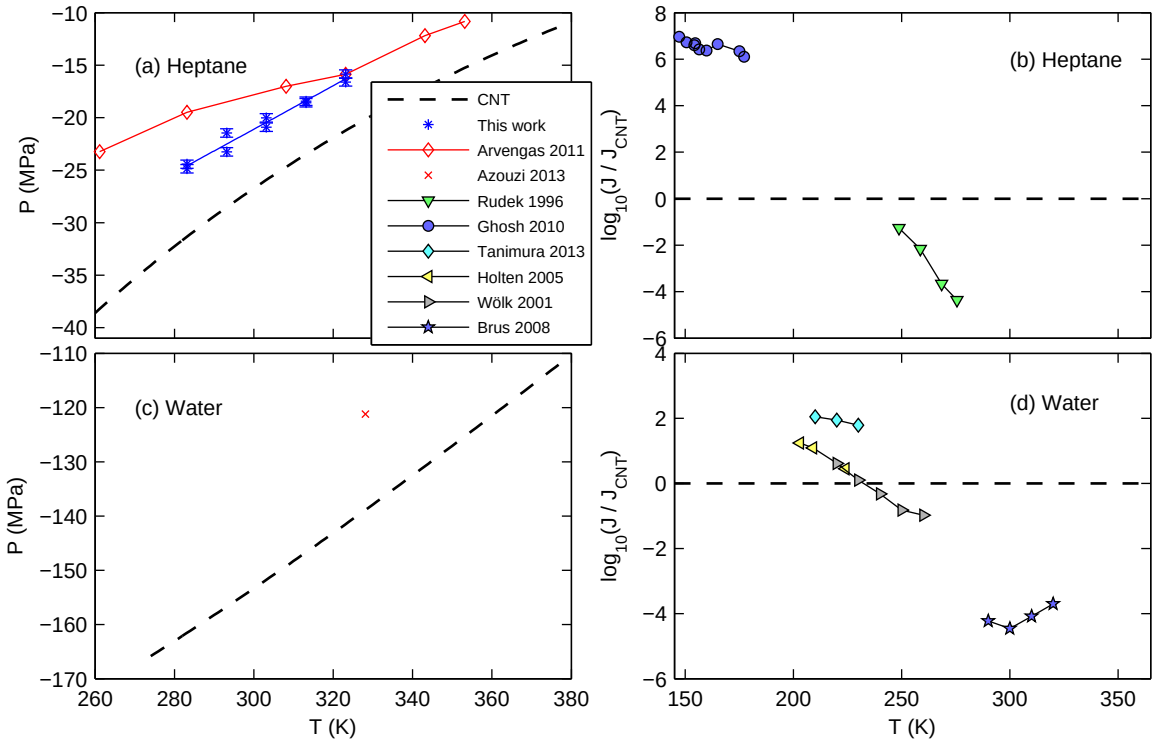

FIG. S1: Same as Fig. 1 in the Letter, but for (a,b) heptane and (c,d) water. The point in (c) corresponds to the cavitation pressure measurement in a water inclusion in a quartz crystal[14].

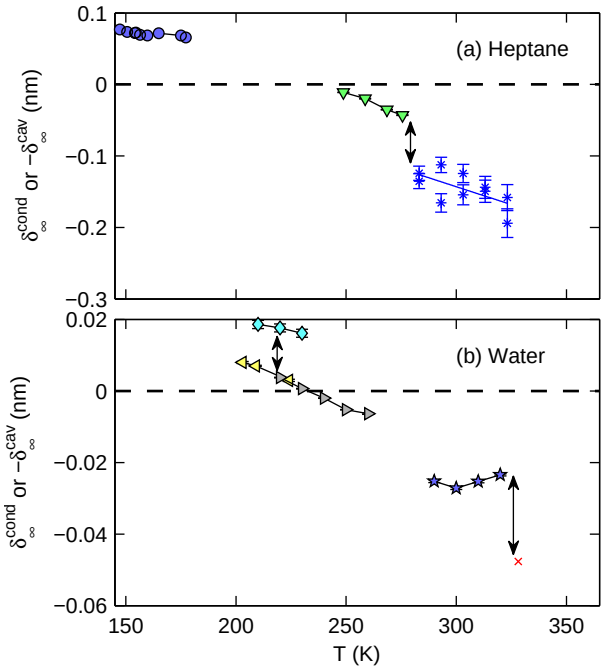

FIG. S2: Same as Fig. 2, but for (a) heptane and (b) water.

B. CNT_2

Eqs. (2), (7) and (9) form a system of equations that can be solved for δ_∞ and $\delta_\infty^2+\alpha$. The relevant solutions are

$$\begin{cases} \delta_\infty &= -\dfrac{R_\mathrm{s}^*}{2}(1-\sqrt{\Delta}) \\ \delta_\infty^2+\alpha &= (R_\mathrm{s}^*)^2\left(\dfrac{2\sigma_\infty}{R_\mathrm{s}^*\Delta P}-\sqrt{\Delta}\right) \end{cases} \tag{S4}$$

where

$$\Delta = 1-\frac{4R_\mathrm{e}^*}{R_\mathrm{s}^*}+\frac{8\sigma_\infty}{R_\mathrm{s}^*\Delta P} \tag{S5}$$

Here, R_e^* is obtained in the experiments from the nucleation theorem and R_s^* is given by Eq. (S1).

C. Choice for the kinetic prefactor

1. Cavitation

The CNT_0 and its variants CNT_1 and CNT_2 rely on the choice of an expression for the kinetic prefactor J_0.

For cavitation, we chose $J_0V\tau = 10^{19}$, where V is the volume where the acoustic wave is focalized, and τ the duration of an acoustic burst. The value is taken from our previous study in water[1]. The actual value of $J_0V\tau$ in the present experiments might differ from the 10^{19} value. However, a change by a factor 10 in this constant only leads to a shift of the experimental points by about 0.015 nm for the CNT_1's δ_∞ and 0.5 nm^3 for V_e^* (for both heptane and ethanol). This is much smaller than the statistical deviations seen by repeating cavitation pressure measurements at the same temperature several times.

2. Condensation

For condensation, the nucleation rates are calculated from the supersaturation $S = P_\mathrm{v}/P_\mathrm{sat}(T)$, where P_v is the pressure of the metastable vapor, and $P_\mathrm{sat}(T)$ is the equilibrium vapor pressure for a flat interface. Treating the vapor as a perfect gas, and the liquid as an incompressible phase leads to:

$$\Delta P = \frac{kT\ln S}{v_\mathrm{l}} \tag{S6}$$

where k is the Boltzmann constant and v_l the volume per molecule in the liquid. (Including gas non-idealities has been shown to have little effect on the nucleation rates for n-nonane[7].) For the kinetic prefactor, we used

$$J_0 = \sqrt{\frac{2\sigma_\infty}{\pi m_\mathrm{l}}}v_\mathrm{l}\,S^2\left(\frac{P_\mathrm{sat}(T)}{kT}\right)^2 \tag{S7}$$

with m_l the mass of a molecule. The actual value of J_0 is still being debated. In particular, a "$1/S$ correction" is sometimes added to Eq. (S7)[6]. This, again, only leads to insignificant changes in the quantities explored in this study. For instance, the typical shifts from the data in[8] are: 2 orders of magnitude for $J_\mathrm{exp}/J_\mathrm{CNT}$, 0.1 nm^3 for V_e^*, 0.02 nm for the CNT_1's δ_∞, and 2×10^{-4} nm and 0.015 nm^2 for the CNT_2's δ_∞ and $\delta_\infty^2+\alpha$.

D. Derivation of the critical volumes from the nucleation theorem

Critical volumes are obtained from the nucleation theorem Eq. (5). When writing Eq. (6) and converting Δn^* into a volume, two consecutive approximations are made. First, we assume that the density at the center of the nucleus is the density of the homogeneous phase, ρ_L or ρ_V. This allows us to link the critical volume to the excess number of molecules by:

$$V_\mathrm{e}^* = \frac{n_\mathrm{e}^*}{\rho_\mathrm{L}} = \frac{\Delta n^*}{\rho_\mathrm{L}-\rho_\mathrm{V}} \quad \text{for droplets} \tag{S8}$$

$$= \frac{n_\mathrm{e}^*}{\rho_\mathrm{V}} = -\frac{\rho_\mathrm{V}}{\rho_\mathrm{L}-\rho_\mathrm{V}}\Delta n^* \quad \text{for bubbles} \tag{S9}$$

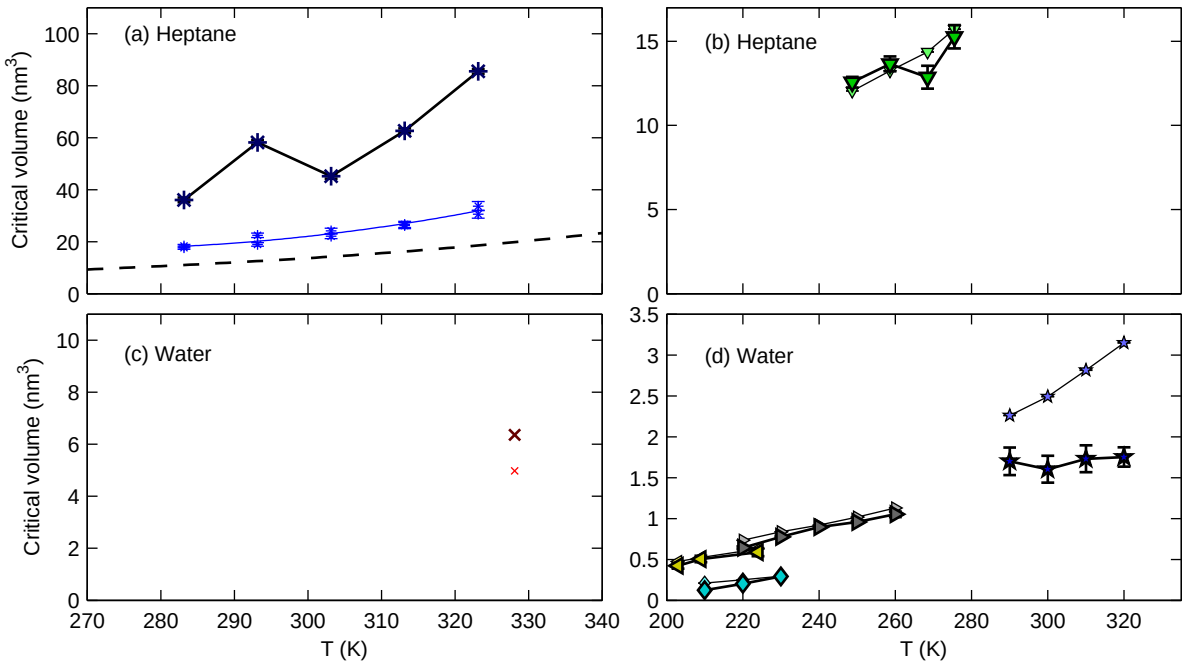

FIG. S3: Same as Fig. 3, but for (a,b) heptane and (c,d) water.

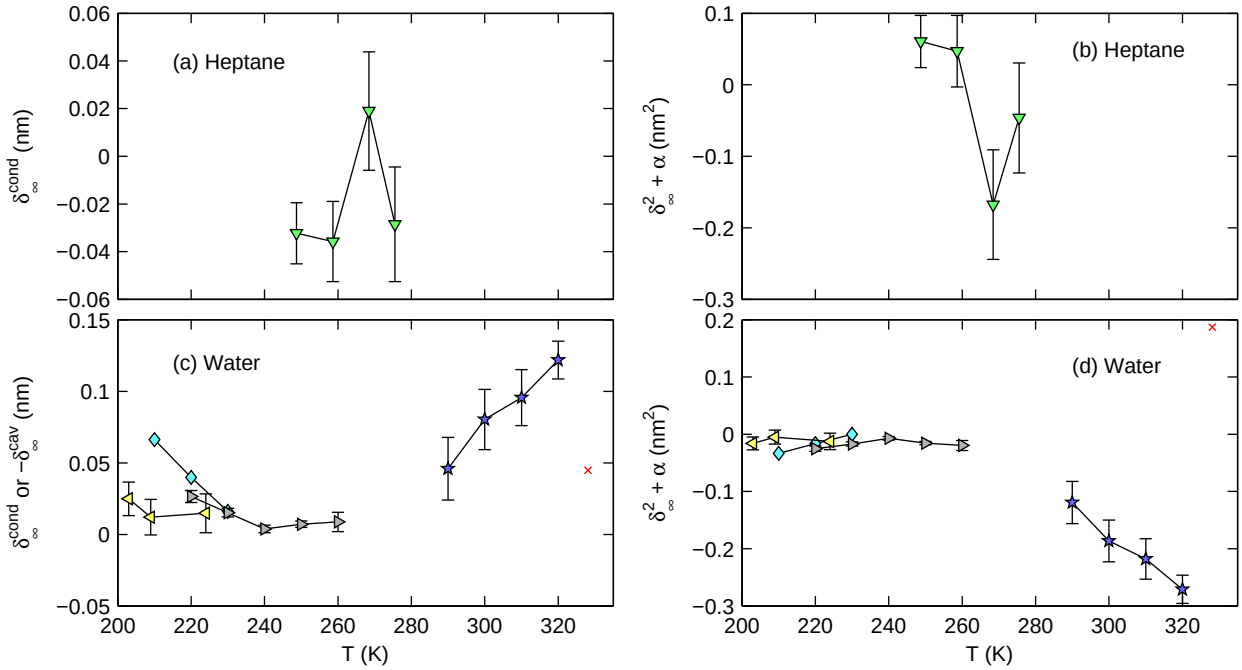

FIG. S4: Same as Fig. 4, but for (a,b) heptane and (c,d) water.

where n_e^* is the number of molecules in the nucleus. The second approximation we make is that $\rho_L \gg \rho_V$, which is easily satisfied: for the data analyzed in the Letter and here, the maximal value of ρ_V/ρ_L is 0.68×10^{-3} for condensation and 1.1×10^{-3} for the FOPH experiments. The critical volume then simply becomes

$$V_e^* = \frac{|\Delta n^*|}{\rho_L} \tag{S10}$$

for droplets and bubbles.

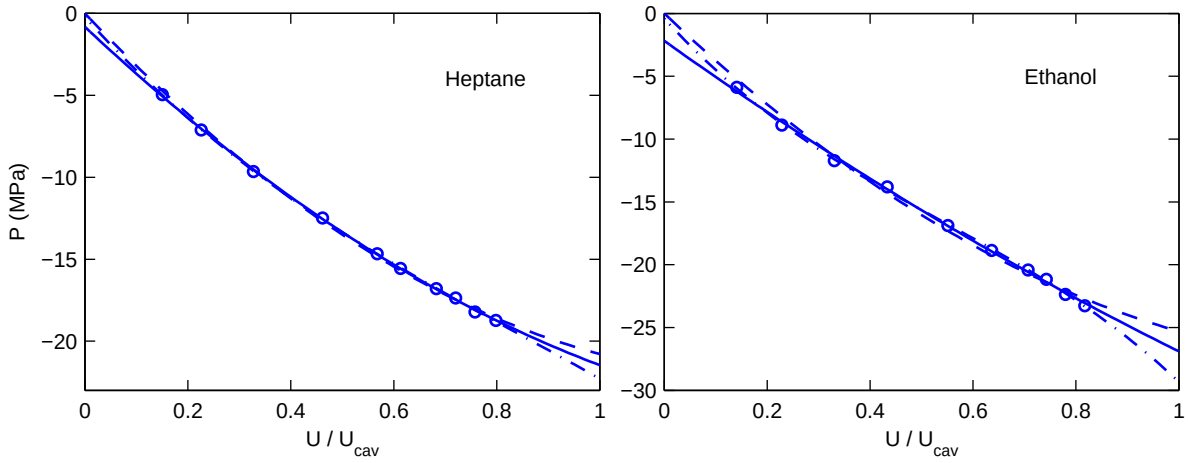

FIG. S5: Pressure depending on the amplitude of the voltage on the piezo-electric transducer for $T = 293$ K. The markers represent the measurements and the lines correspond to the different polynomials used to extrapolate the curve up to $U = U_{\rm cav}$: P_1 (dashed line), P_2 (solid line) and P_3 (dash-dotted line).

The two approximations above lead to an underestimate of the critical volumes[9,10]. Correcting for these would therefore make the discrepancy between the real critical volumes and the CNT_1's volumes that we highlight in the main text stronger.

V. EFFECT OF THE EXTRAPOLATION OF THE VOLTAGE TO PRESSURE RELATION (CAVITATION EXPERIMENTS)

A large part of the uncertainties in our experiments do not come from statistical error bars. To measure the cavitation pressures and the critical volumes in the fiber-optic probe hydrophone experiments, pressures are measured for different amplitudes of the sound wave created by a piezo-electric transducer. The amplitude is controlled by the amplitude of the oscillatory voltage U applied to the transducer (see Ref. 3 for details on the setup). Unfortunately, the voltage cannot be increased up to the value for which there would be 50 % chance to cavitate as it would damage the end facet of the fiber. To obtain the pressure $P_{\rm cav}$ at the voltage $U_{\rm cav}$, the pressure is measured for several values of U below about $0.8U_{\rm cav}$, and we fit the data with some function to extrapolate the pressures to $P_{\rm cav}$. We have tried several functions for the extrapolation, and three of them gave sufficiently small residuals:

$$P_1(U) = a_2U^2 + a_1U\,, \tag{S11}$$

$$P_2(U) = b_2U^2 + b_1U + b_0 \tag{S12}$$

and

$$P_3(U) = c_3U^3 + c_2U^2 + c_1U + c_0 \tag{S13}$$

where the a_i, b_i and c_i are the fitting coefficients. We show the three extrapolations for a given temperature in heptane and ethanol in Fig. S5. On this plot, $P_{\rm cav}$ can simply be read for $U = U_{\rm cav}$. To calculate the critical volumes from the nucleation theorem within the framework of CNT_1, Eq. (6) is rewritten in terms of a derivative $\partial P/\partial U$ of the pressure with the voltage, so that the critical volumes are related to the slope of $P(U)$ at $U_{\rm cav}$. Since we could not find any strong argument to determine which extrapolation is the best, we display in Figs. S6, S7 and S8 the quantities obtained with the three polynomials. The graphs of the main text (and their equivalents for heptane and water in Figs. S1, S2, S3 and S4) use polynomial P_2 as its residuals were slightly better than for the other functions and because it often lies between the values computed with P_1 and P_3. The choice of the function for the extrapolation can lead to significant changes of the various quantities plotted, especially the critical volumes. However, no matter what function is used, there is no master curve emerging in Fig. S7 (for heptane), and it appears very unlikely from Fig. S8 that the real critical volumes from the nucleation theorem could match the volumes from the CNT_1.

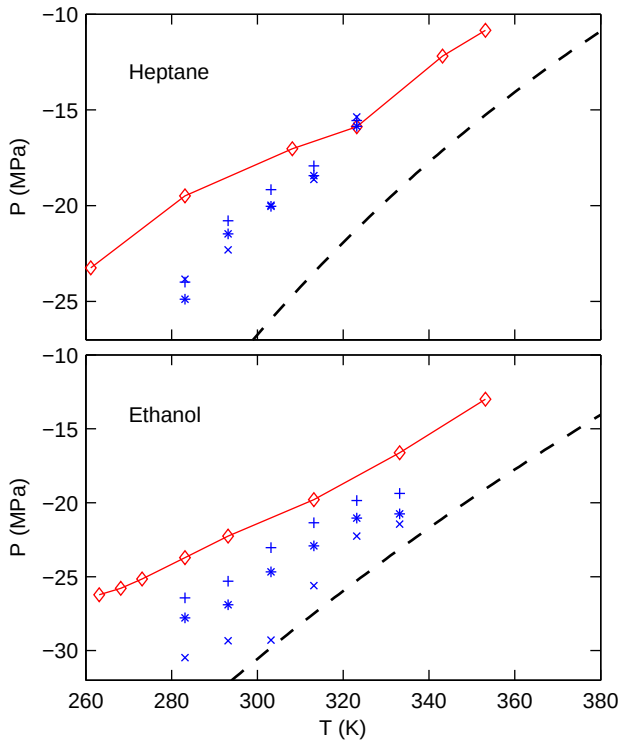

FIG. S6: Same as in Figs. 1 and S1 for one of the two FOPH series of measurements, but showing the results from the three functions P_1 (+ markers), P_2 (∗ markers) and P_3 (× markers).

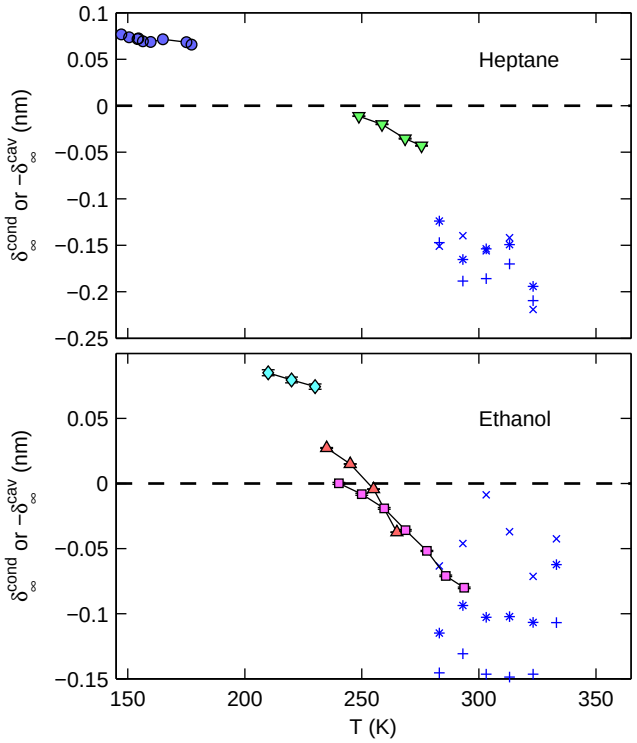

FIG. S7: Same as in Figs. 2 and S2 for one of the two FOPH series of measurements, but showing the results from the three functions P_1 (+ markers), P_2 (∗ markers) and P_3 (× markers).

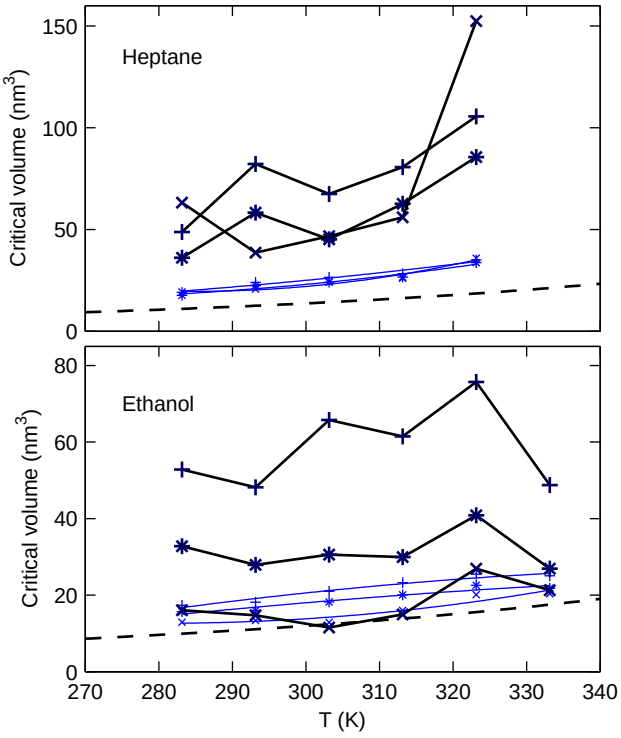

FIG. S8: Same as in Figs. 3 and S3, but showing the results from the three functions P_1 (+ markers), P_2 ($*$ markers) and P_3 ($\times$ markers).

VI. CNT_2 FOR CAVITATION

Cavitation data have been omitted in the CNT_2 analysis. The reason is that increasing the order also increases the error bars, and the errors induced by the $P(U)$ extrapolation (see above) lead to a large uncertainty in δ_∞ and $\delta_\infty^2 + \alpha$. Moreover, the values of the cavitation pressures and of the critical volumes are such that the solving of the second order polynomial to obtain the solutions in Eq. (S4) sometimes gives no real roots. Fig. S9 shows the cavitation analysis for the points that do have a solution, along with the condensation experiments. The systematic error induced by the choice of the $P(U)$ relation is typically of the order of the range of the y axis of the graphs for both δ_∞ and $\delta_\infty^2 + \alpha$.

VII. ESTIMATE OF THE STATISTICAL ERROR BARS

Whenever it was possible, we have put statistical error bars on the quantities δ_∞ and V_e^* from CNT_1, V_e^* from the NT, and δ_∞ and $\delta_\infty^2 + \alpha$ from the CNT_2. This section describes how they were calculated.

A. Fiber-optic probe hydrophone experiments

In the fiber-optic probe hydrophone (FOPH) experiments, the error bars in $\delta_\infty^{\mathrm{cav}}$ have been estimated on repeated experiments at a single temperature, $T = 293$ K. Between two cavitation pressure measurements, the fiber was removed and repositioned at the acoustic focal point. The results were dispersed with a standard deviation of 0.4 MPa, which we took as the error bar for all temperatures. To complement this statistical error, we also display, in the Letter and here, the FOPH measurements in heptane and ethanol for two series of temperatures (for each liquid). When switching to a new series, the fiber was cleaved to renew its end facet, which leads to an additional uncertainty in the measurements.

The critical volumes from the nucleation theorem V_e^* rely on a nonlinear fit of the probability to cavitate $\Sigma(U)$, with one of the parameters, ξ, representing the "width" of the $\Sigma(U)$ curve that has an "S" shape[2]. The error bar on ξ has been estimated for each liquid for a single temperature. Assuming that the experiment gave a set of points

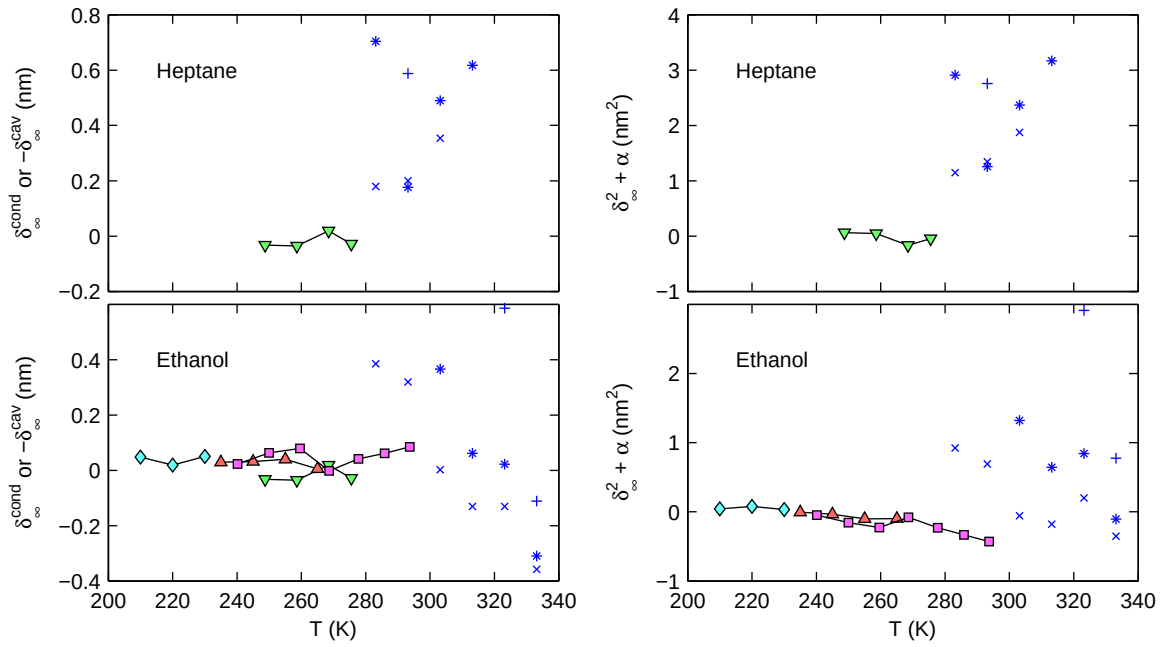

FIG. S9: Same as Figs. 4 and S4, but including the cavitation points with polynomial P_1 (+ markers), P_2 ($*$ markers) and P_3 ($\times$ markers).

$\{(U_{\rm exp}, \Sigma_{\rm exp})_i\}$, we have generated numerically several sets $\{(U_{\rm exp}, \Sigma_{\rm num})_i\}$ and fitted an S-curve on each of them, thus providing us with a standard error on ξ. The generation of a given point $(U_{\rm exp}, \Sigma_{\rm num})$ is done by taking for $\Sigma_{\rm num}$ a random value corresponding to the average of N values $\sigma_j \in \{0, 1\}$ with a probability of obtaining 1 equals to $\Sigma_{\rm exp}$.

B. Condensation experiments

The condensation data typically correspond to measurements of the nucleation rate J for different values of the supersaturation S, and of the temperature T. For a given temperature, the $S(J)$ curve is expected to be a portion of a line, and such a fit is indeed performed to obtain the critical volume $V_{\rm e}^*$. We extract two statistical errors from that fit:

- The standard error on the slope.
- A standard error on the average nucleation rate for the given temperature. When plotting the $S(J)$ fit function together with the experimental points, these are dispersed around the fit function. Assuming that there is an error in the J measurements, but that S is known precisely, this allows to estimate an overall statistical error in a single J measurement, ΔJ_0, from the deviation of the experimental J to the fit function.

These made possible the calculation of standard errors on the following quantities:

- The first error above is used to get the statistical error on $V_{\rm e}^*$ (from nucleation theorem).
- Since we used, for a given temperature, the average value (over all S) of J as an input in the δ_∞ and $V_{\rm e}^*$ formulas, the standard errors on these quantities simply derive from the standard error $\Delta J = \Delta J_0/\sqrt{N}$, with N the number of points for the fit.
- The δ_∞ and $\delta_\infty^2 + \alpha$ quantities both depend on the two parameters J and $V_{\rm e}^*$. We have noted that in most of the cases the error due to J in δ_∞ and $\delta_\infty^2 + \alpha$ is at least 10 times smaller than the error due to $V_{\rm e}^*$. We have therefore only included the standard error due to the critical volumes in δ_∞ and $\delta_\infty^2 + \alpha$.

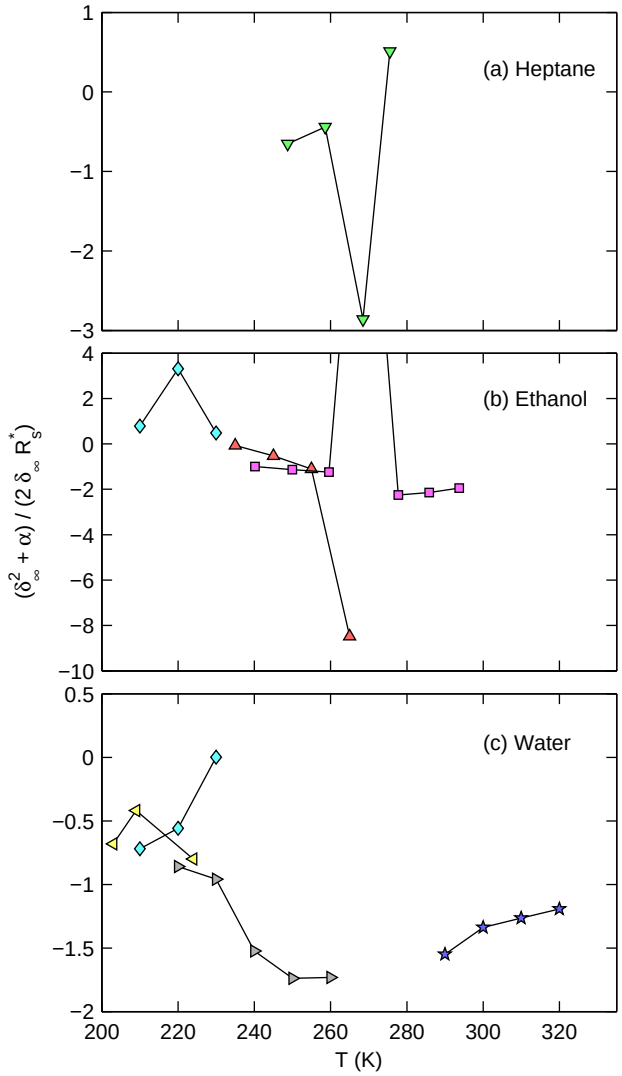

FIG. S10: Ratio between the second order term $(\delta_\infty^2 + \alpha)/(R_s^*)^2$ and the first order term $2\delta_\infty/R_s^*$. The point out of the graph for ethanol is at a height $(\delta_\infty^2 + \alpha)/(2\delta_\infty R_s^*) = 269$.

VIII. SECOND ORDER APPROXIMATION FOR THE SURFACE TENSION σ_s

A. Validity

Eq. (9) is derived by Taylor expanding and integrating the Gibbs-Tolman-Koenig-Buff (GTKB) equation (Eq. (26) in Ref. 11) to second order in $1/R_s^*$, by neglecting terms such as $\delta_\infty^3/(R_s^*)^3$ and $\alpha^2/(R_s^*)^4$. For each pair of values $(\delta_\infty, \delta_\infty^2 + \alpha)$ from the experiments, we have compared the value of σ_s from Eq. (9) with the full numerical integration of the GTKB equation. For the 34 points used to plot Figs. 4 and S4, the maximum relative error is 3.7 %, and 29 points give an error of less than 1 %, which makes Eq. (9) an excellent approximation for realistic ranges of parameters for condensation.

B. Comparison of the two terms in the σ_s expansion of the CNT_2

With the beginning of the use of models including a second order related to the rigidity of the interface, some debate emerged about the relative amplitudes of the two terms $2\delta_\infty/R_s^*$ and $(\delta_\infty^2 + \alpha)/(R_s^*)^2$. In simulations, models that include the second term only, or that include the two terms[12,13] have been tested. For the experiments, their ratio,

extracted from the condensation measurements, is shown in Fig. S10. Overall, we found that the two quantities are often of the same order of magnitude. Sometimes, the ratio takes values much larger than 1, but this only happens when δ_∞ is very close to 0, so that these points may have large error bars, because of the error in the δ_∞ values. Therefore, we expect that a model of a surface tension varying as $\sigma_\infty/\sigma_\mathrm{s} = 1 + C/(R_\mathrm{s}^*)^2$, with C a constant, would display inconsistencies similar to those found with the CNT_1 model.

IX. FITTED CNT_2 PARAMETERS FOR ETHANOL

Considering the condensation data only, we obtained an overall agreement of all the data in the sense that the points are closer to master curves for $\delta_\infty(T)$ and $(\delta_\infty^2 + \alpha)(T)$ in the CNT_2 than what was found for δ_∞ in the CNT_1. The best results are obtained for ethanol. We have fitted in this case these functions by simple expressions that can be used as empirical functions, namely a constant δ_∞ and a linear $\delta_\infty^2 + \alpha$:

$$\delta_\infty^2 + \alpha = A(T - T_\mathrm{ref}) + B \tag{S14}$$

With $T_\mathrm{ref} = 298.15$ K, the fit parameters are $\delta_\infty = 0.04095$ nm, $A = -0.005460$ nm^2/K and $B = -0.3352$ nm^2.

[1] E. Herbert, S. Balibar, and F. Caupin, "Cavitation pressure in water," *Phys. Rev. E*, vol. 74, p. 041603, 2006.

[2] A. Arvengas, E. Herbert, S. Cersoy, K. Davitt, and F. Caupin, "Cavitation in heavy water and other liquids," *J. Phys. Chem. B*, vol. 115, pp. 14240–14245, 2011.

[3] A. Arvengas, K. Davitt, and F. Caupin, "Fiber optic probe hydrophone for the study of acoustic cavitation in water," *Rev. Sci. Instrum.*, vol. 82, p. 034904, 2011.

[4] C. Appert, C. Tenaud, X. Chavanne, S. Balibar, F. Caupin, and D. d'Humiéres, "Nonlinear effects and shock formation in the focusing of a spherical acoustic wave," *Eur. Phys. J. B*, vol. 35, pp. 531–549, 2003.

[5] K. Davitt, E. Rolley, F. Caupin, A. Arvengas, and S. Balibar, "Equation of state of water under negative pressure," *J. Chem. Phys.*, vol. 133, pp. –, 2010.

[6] V. Holten, D. G. Labetski, and M. E. H. van Dongen, "Homogeneous nucleation of water between 200 and 240 K: New wave tube data and estimation of the tolman length," *J. Chem. Phys.*, vol. 123, p. 104505, 2005.

[7] J. A. Fisk and J. L. Katz, "Condensation of supersaturated vapors. x. pressure and nonideal gas effects," *J. Chem. Phys.*, vol. 104, pp. 8649–8656, 1996.

[8] S. Tanimura, H. Pathak, and B. E. Wyslouzil, "Binary nucleation rates for ethanol/water mixtures in supersonic laval nozzles: Analyses by the first and second nucleation theorems," *J. Chem. Phys.*, vol. 139, p. 174311, 2013.

[9] D. W. Oxtoby, "Nucleation of first-order phase transitions," *Acc. Chem. Res.*, vol. 31, pp. 91–97, 1998.

[10] D. Kashchiev, "Thermodynamically consistent description of the work to form a nucleus of any size," *J. Chem. Phys.*, vol. 118, pp. 1837–1851, 2003.

[11] A. Tröster, M. Oettel, B. Block, P. Virnau, and K. Binder, "Numerical approaches to determine the interface tension of curved interfaces from free energy calculations," *J. Chem. Phys.*, vol. 136, p. 064709, 2012.

[12] B. J. Block, S. K. Das, M. Oettel, P. Virnau, and K. Binder, "Curvature dependence of surface free energy of liquid drops and bubbles: A simulation study," *J. Chem. Phys.*, vol. 133, p. 154702, 2010.

[13] V. G. Baidakov and K. S. Bobrov, "Spontaneous cavitation in a lennard-jones liquid at negative pressures," *J. Chem. Phys.*, vol. 140, p. 184506, 2014.

[14] M. E. M. Azouzi, C. Ramboz, J.-F. Lenain, and F. Caupin, "A coherent picture of water at extreme negative pressure," *Nat. Phys.*, vol. 9, pp. 38–41, 2013.